8th International Symposium on Magnetic Bearing
August 26-28, 2002, Mito, Japan

CONTROL OF FLEXIBLE ROTORS SUPPORTED BY ACTIVE MAGNETIC BEARINGS

Hiroyuki Fujiwara
Dept. of Mechanical Eng., National Defense Academy, Yokosuka, Kangawa, 239-8686, Japan
hiroyuki@nda.ac.jp
Koji Ebina
Dept. of Mechanical Eng., National Defense Academy, Yokosuka, Kangawa, 239-8686, Japan
Makoto Ito
Dept. of Mechanical Eng., National Defense Academy, Yokosuka, Kangawa, 239-8686, Japan
g410063@nda.ac.jp
Naohiko Takahashi
Hitachi Industries Co. Ltd., Tsuchiura, Ibaraki, 300-0013, Japan
naohiko_takahashi@pis.hitachi.co.jp
Osami Matsushita
Dept. of Mechanical Eng., National Defense Academy, Yokosuka, Kangawa, 239-8686, Japan
osami@nda.ac.jp

ABSTRACT

In the design of control networks operating AMB, consideration of strong levitation stiffness and enough damping to pass critical speeds of flexible rotors is paramount for successful operation. In order to assign the stiffness and damping properties for rigid and flexible modes ranging in the rated rotational speed, the optimization of these properties is easily influenced by the occurrence of high frequency instability of bending mode instability, called spill-over instability. This paper treats two cases of an analog and digital controls. In the former case, we recommend PID plus a phase bump filter which works for anti-spill-over. The corresponding rotational test proved its effectiveness. In the latter case, control via mode control concerning translating and tilting vibrations was employed. Since several case studies were executed, design of a PID plus a notch filter for the translating system and PID plus a phase shifting filter for the tilting system, respectively was used. The stability margin is measured by a open loop transfer function and positive evaluation was obtained. The rotational test without instability was achieved by passing the second bending mode critical speed up to the rated speed of 250 rps.

1. INTRODUCTION

Active Magnetic Bearings (AMB), which utilize magnetic levitation technology, have recently been applied to industrial rotors [1]. The AMB levitate the rotor by feedback control without mechanical contact. In the design of control networks operating AMB, which are used in the levitation of flexible rotors, the damping properties for rigid and flexible modes ranging in the operating speed must be considered. However, this optimization easily induces high order bending mode instability, because a rotor has many eigen modes. Therefore, the controller is needed for stabilizing the instability of high order bending modes, which is called spill-over instability. This spill-over instability has been a research task of rotating machinery [2].

In the first step of this paper, the discussion of an analog control using a conventional PID plus a phase bump filter which enables the anti-spill-over in very high frequency range(0- 1.5KHz) is reviewed. This method was evaluated by the rotational test.

Second, discussion move to the use of a digital controller. In this case, it was impossible to extend the phase lead up to such very high frequencies. Instead, a notch filter or a phase shifting filter with the combination of PID were introduced. These additional filters work by compensating spill-over instability of high frequency regions. Simultaneously, the rotor control system is modeled by using the mode control method which controls the rotor vibration respectively and independently in the translating and tilting modes. The PID plus a notch filter in the translating mode control and PID plus a phase shifting filter in tilting systems are utilized. As a result, the effects of the controller are demonstrated by the evaluation of stability margin at standstill, and show that the rotational speed of the test rotor exceeded the frequency of the 2nd bending mode in a running test without any instability.

2. EXPERIMENTAL SYSTEM

Figure 1 shows the outline of an experimental system. The experimental system consists of a flexible rotor, two radial AMBs, a non-contact, flat and built-in motor (left side), a thrust AMB (right side) and a vacuum chamber. This AMB rotor system is categorized in 5 axes control. The system is operated in the vacuum chamber (about 0.5 Torr) in order to prevent air loss.

The radial and thrust AMBs are constructed as half-split type, as shown in Figure 2, to allow for easy reassembly and the maintenance.

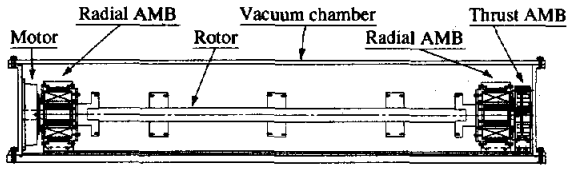

FIGURE 1: Outline of experimental system

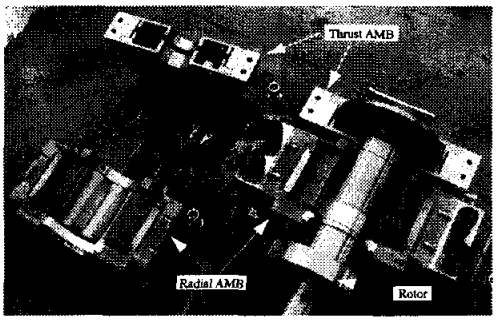

FIGURE 2: Split type of AMB

3. A FLEXIBLE ROTOR

3.1 Structure of flexible rotor

Figure 3 shows the structure of the flexible rotor used in our experiment. There are three fat discs at the center and two end plates. The left end plate is a motor rotor, and the right end plate is a thrust AMB rotor. The AMBs are arranged on both sides with the bearing span of 1195 mm. Table 1 shows the specification of this flexible rotor.

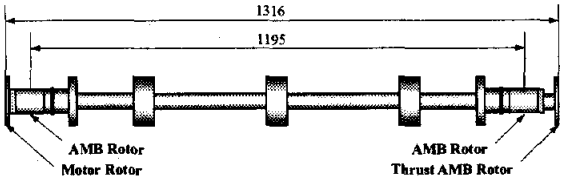

FIGURE 3: Structure of flexible rotor

TABLE 1: Specification of rotor

mass	31.4 (kg)
diameter×span	ϕ37×1316 (mm)
material	SUS304
rated speed	250 (rps)

3.2 Critical speed map

The critical speed map of the flexible rotor is shown in Figure 4. The horizontal and vertical axes are the support stiffness and the natural frequency of the flexible rotor, respectively. On the map, the natural frequency drawn at the left end corresponds to the free-free boundary condition and the natural frequency located at the right end is closed to pin-pin boundary condition.

These solid curves are the natural frequency of each eigen mode of the flexible rotor at standstill. The dotted line is the predicted value of the AMB support stiffness expected. The intersections between these natural frequency curves and the AMB stiffness line indicate the critical speeds, noted Nci (i=1-7), which are predicted unbalance resonance speeds during the rotation.

There are four critical speeds up to the rated rotational speed (250rps). The first two, noted by Nc1 and Nc2, are rigid modes. The other modes, noted by Nc3 and Nc4 are bending modes which we must pass to reach the rated speed. Figure 5 shows the corresponding eigen mode shapes of rigid and bending critical speeds.

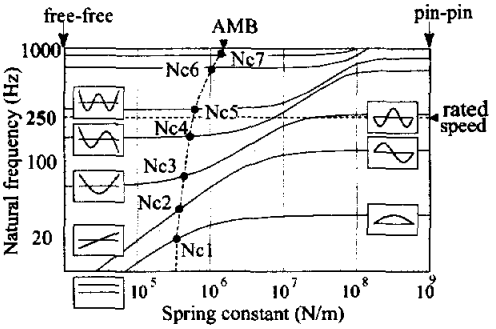

FIGURE 4: Critical speed map

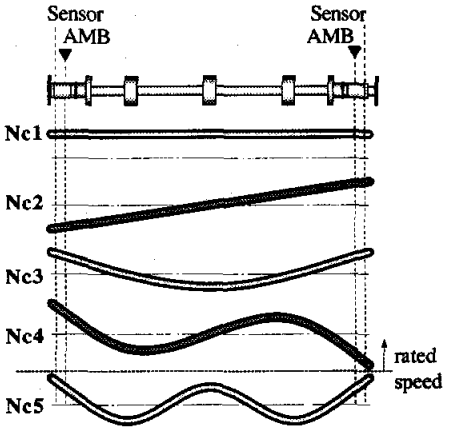

FIGURE 5: Eigen modes

4. ANALOG CONTROL OPERATION

4.1 Analog control

The analog control for the experimental operation was considered. The controller was based on the PID control plus a phase bump filter (PBF). The phase bump filter was added to countermeasure spill-over instability of high frequency mode[3]. The transfer function of this PBF is expressed in mathematics:

$$G_{PBF} = \frac{1}{1-\alpha}\left(1 - \frac{\alpha}{(\tau s)^2 + 2\zeta\tau s + 1}\right) \qquad (1)$$

The corresponding Bode and Nyquist plots are drawn in Figure 6. The phase bump filter provides the feature where phase lead largely increases with minimal increase in gain, as shown nearby about ω=1 of Figure 6. The increase of phase lead looks bump behavior.
By using this analog controller (PID+PBF), the phase lead of this analog controller extends to 1500Hz as shown in Figure 7.

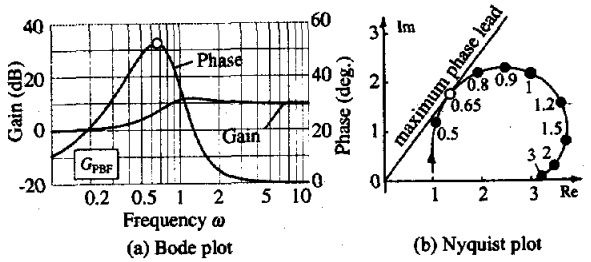

(a) Bode plot (b) Nyquist plot

FIGURE 6: Phase bump filter

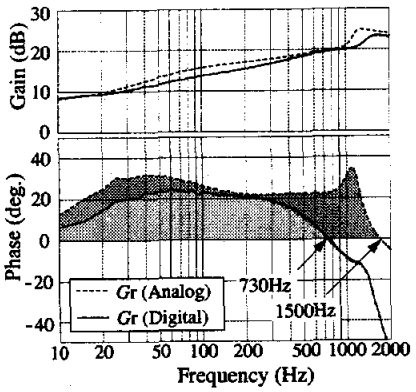

FIGURE 7: Bode plot of controller (PID+PBF)

4.2 Rotational test

With the analog controller completed, rotation testing was conducted. In this case, the rotor configuration was the same as Figure 1, but the rotor was mechanically connected with the motor by a flexible coupling. Through experimentation with the analog controller and the repeat balancing of the rotor, rotor speed beyond the 1st bending critical speed of Nc3 was accomplished without the instability, as shown in Figure 8.

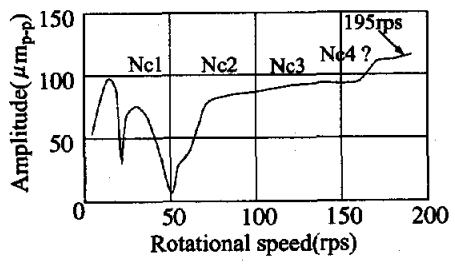

FIGURE 8: Rotation test (Analog control)

However, when the rotor reached maximum speed of 190 rps before the rated speed of 250 rps, the flexible coupling broke down. At this maximum speed, near the second bending critical speed, Nc4, large vibrations were observed making it impossible to continue higher rotational speeds. For this reason the system was modified to a non-contact flat motor. Simultaneously, the controller was changed from the analog type to a digital type as discussed in the following section.

5. DIGITAL CONTROL OPERATION

5.1 Phase lag due to digitalization

The analog controller was replaced by a digital controller using s-z transformation including the algorithm of the phase bump filter. The sampling frequency is 20kHz. Through experimentation, the measurement and comparison of the transfer functions of both analog and digital controllers were obtained, as shown in Figure 7. In the case of the digital controller, the phase lead region on the Bode plot decreases from 1500Hz down to 750Hz. This decrease of the maximum frequency to guarantee the phase lead is caused by a digitalization, mainly due to the phase lag of the hold circuit.
As predicted, the digital controller stabilize the system to eliminate instability of the high frequency mode due to the spill-over problem.

5.2 Mode control method

A mode control method for the control of the AMB equipped rotor was now employed. In the case of mode control, as shown in Figure 9, both displacement signals detected at the left and right AMBs are converted to parallel and tilting modal displacements, and the control is then conducted in modal coordinates.
Figure 9(a) shows the algorithm of the mode control in the X-direction. The Y-directional control layout is same as the X-direction.
The displacement signals (x_1 , x_2) come from both AMBs to the separator. The separator divides input signals (x_1 , x_2) into mode signals (x_p , x_t), i.e., parallel mode displacement x_p and tilting mode displacement x_t , respectively, according to the following equation:

$$\begin{pmatrix} x_p \\ x_t \end{pmatrix} = \frac{1}{2}\begin{pmatrix} 1 & 1 \\ 1 & -1 \end{pmatrix}\begin{pmatrix} x_1 \\ x_2 \end{pmatrix} \qquad (2)$$

Each mode controller individually produces the output voltages, as follows:

$$v_p = G_{rp}(s)x_p \quad v_t = G_{rt}(s)x_t \qquad (3)$$

These outputs (v_p, v_t) is recomposed to side 1 and side 2 commands (v_1 , v_2) :

$$\begin{pmatrix} v_1 \\ v_2 \end{pmatrix} = \begin{pmatrix} 1 & -1 \\ 1 & 1 \end{pmatrix} \begin{pmatrix} v_p \\ v_t \end{pmatrix} \quad (4)$$

According to these commands, the power amplifiers supply the current in AMB coils in each side 1and side 2. This is a global description of the mode control layout.

In fact, the calculation of these equations is executed by DSP –PC system as indicated in a block diagram of the mode control method as shown in Figure 9 (b).

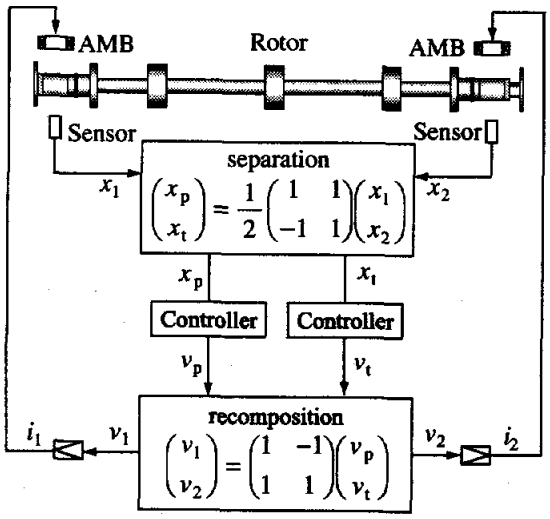

(a) Mode control layout

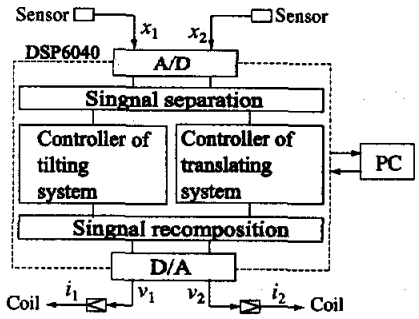

(b) DSP and PC system

FIGURE 9: Mode control and digital equipment

Consequently, a set of the AMB sensor signal is separated to the translating system and tilting system by a signal separator. As being obviously understood from the combination of Figure 5 and 9, the following control strategy is accepted:

parallel mode controller $G_{rp}(s)$ controls

translating rigid mode Nc1,

Bending modes Nc3, Nc5... , and

tilting mode controller $G_{rt}(s)$ controls

tilting rigid mode Nc2,

Bending modes Nc4, Nc6...

5.3 Plant transfer function

Determination of the plant transfer function for the controller design is now required. This function can be measured by means of the network shown in Figure 10 with indicated measuring points. In the Figure 10, the points (①, ①') is a swept sin input. The open loop transfer function of the plant except the controller can be identified by the measurement of G_{pp}=③/② as the translating plant system, and G_{pt}=③'/②' as the tilting plant system.

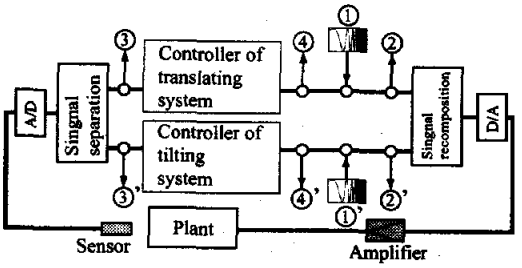

FIGURE 10: Open loop transfer function of plant

The result of these plant transfer functions are shown in Figure 11. In the Figure 11(a), the gain curve of the translating plant transfer function (open loop transfer function except the controller in the translating network), noted G_{pp}=③/② is shown. In this case, the peaks of gain appear at Nc3, Nc5 and Nc7 of the natural frequency of the rotor. On the other hand, in the Figure 11(b) showing the tilting plant transfer function G_{pt}=③'/②', the peaks of gain at Nc4 and Nc6 are observed.

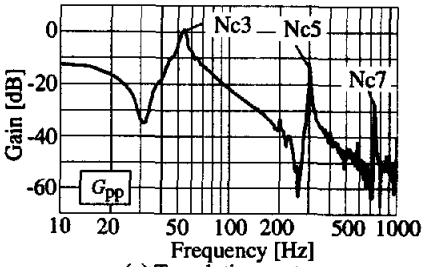

(a) Translating system

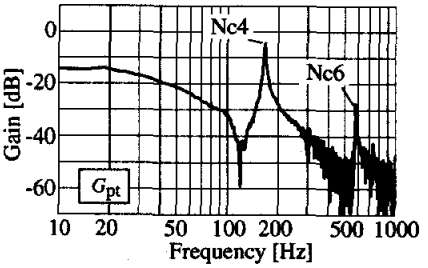

(b) Tilting system

FIGURE 11: Plant transfer function

Mode separation is completed in this manner. Since each plant system is independently identified, controller design for translating and tilting system by using mode control is simple.

5.4 Digital controller with anti-spill-over

Generally, spill-over instability has been avoided by using a notch filter (NF), as expressed in following mathematics:

$$G_{NF} = \frac{1-(\tau s)^2}{1+2\zeta\tau s+(\tau s)^2} \qquad (5)$$

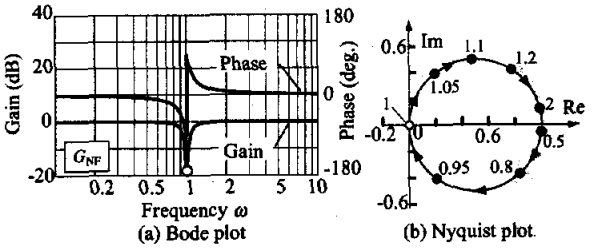

(a) Bode plot (b) Nyquist plot

FIGURE 12: Notch filter

This filter is used to suppress the sensitivity of high frequency modes. The corresponding Bode and Nyquist plots are drawn in Figure 12. This is a very popular means for stabilization. By using this filter in combination with PID in translating mode control, so as G_{rp}= PID+NF .

An attempt was made to insert notch filter also in the titling system. However, this did not work well. Instead the adoption of a PID plus a phase shifting filter (PSF) was utilized. The transfer function PSF is expressed in the following equation.

$$G_{PSF} = \frac{(\tau_2 s)^2 - 2\zeta_2(\tau_2 s)+1}{(\tau_1 s)^2 + 2\zeta_1(\tau_1 s)+1} \qquad (6)$$

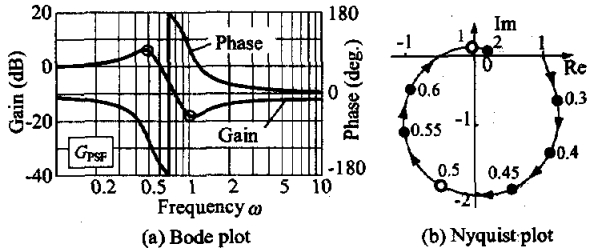

(a) Bode plot (b) Nyquist plot

FIGURE 13: Frequency analysis of phase shifting filter

Figure 13(a) shows the Bode plot of the phase shifting filter, and the corresponding Nyquist plot. The phase lag of the transfer function is over 180 degrees and close to 360 degrees asymptotically. The transfer function is designed for having the phase lag of 270 degrees at the natural frequency of the rotor. The phase lag of 270 degrees is equivalent to the phase lead of 90 degrees. The controller with this filter potentially provides sufficient damping against resonance vibrations.

5.5 Design of mode controller

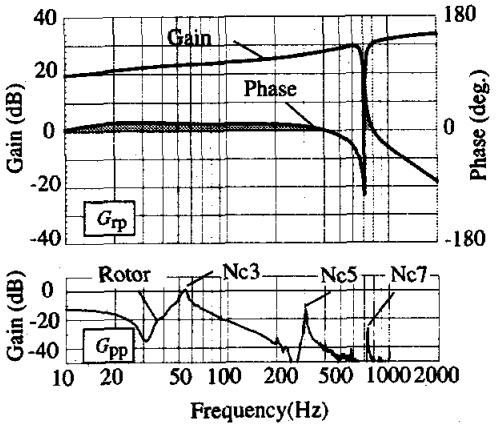

$$G_{rp} = \left(\frac{100}{\tau_1 s+1} + \frac{\tau_2 s+1}{\alpha_1\tau_2 s+1} + \frac{\tau_3 s+1}{\alpha_2\tau_3 s+1}\right)\frac{(\tau_4 s)^2+1}{(\tau_4 s)^2+2\zeta_1(\tau_4 s)+1}$$

$\tau_1 = 1/(2\pi 0.15)$, $\tau_2 = 1/(2\pi 10)$, $\alpha_1 = 0.4$, $\tau_3 = 1/(2\pi 100)$, $\alpha_2 = 0.075$, $\tau_4 = 1/(2\pi 710)$, $\zeta_1 = 0.05$

(a) Translating controller system

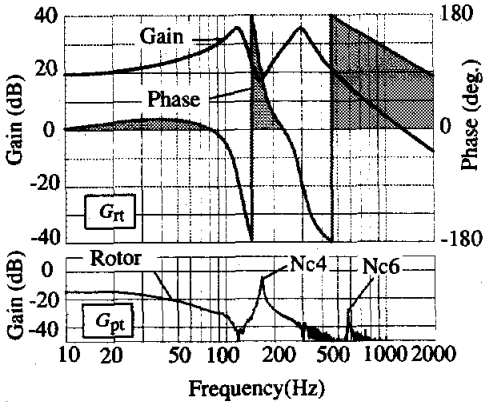

$$G_{rt} = \left(\frac{100}{\tau_5 s+1} + \frac{\tau_6 s+1}{\alpha_3\tau_6 s+1}\right)\frac{(\tau_7 s)^2 - 2\zeta_2(\tau_7 s)+1}{(\tau_8 s)^2+2\zeta_3(\tau_8 s)+1}\,\frac{1}{(\tau_9 s)^2+2\zeta_4(\tau_9 s)+1}$$

$\tau_5 = 1/(2\pi 0.15)$, $\tau_6 = 1/(2\pi 35)$, $\alpha_3 = 0.376$, $\tau_7 = 1/(2\pi 163)$, $\tau_8 = 1/(2\pi 123)$, $\zeta_2 = 0.084$, $\zeta_3 = 0.109$, $\tau_9 = 1/(2\pi 300)$, $\zeta_4 = 0.12$

(b) Titling controller system

FIGURE 14: Bode plot of the controller and gain curves of plant

Control for AMBs was conducted by using the plant transfer functions shown in Figure 11.

For the translating mode control, a combination of PID + Notch filter was created with small revisions. The final configuration was completed as shown in Figure

14(a). Each bending mode peak, Nc3, Nc5 and NC7, is designed to be located within the phase lead domain, and these modes will be then stable.
For the titling mode control, a combination type of PID + Phase shifting filter was designed with additional refinement through simulation. The final configuration is completed as shown in Figure 14(b). Each bending mode peak, Nc4 and Nc6, is well designed to be located within the phase lead domain. These modes are now stable.

5.6 Stability margin

To confirm the stability margin experimentation was performed. Figure 15(a) shows the Nyquist plot of the open loop transfer function for the translating system, i.e., G_{op}=④/② shown in Figure 10. In the same way, Figure15(b) is the open loop transfer function for the tilting system of G_{ot}=④'/②' shown in Figure 10. In Figure 15, the upper and lower plots are stabilized due to the notch filter and the phase shift filter for the spill-over frequency, respectively. We can measure the shortest distance between the Nyquist plot locus and the critical point (-1, 0) which is reverse proportional to the stability margin. Longer distance is required for more stability. By comparing these two plots it can be shown that the tilting system (the lower plot) is more stable than the translating system (the upper plot). The effectiveness of the phase shifting filter is confirmed by the comparison.

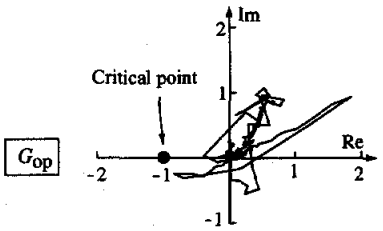

(a) Translating system

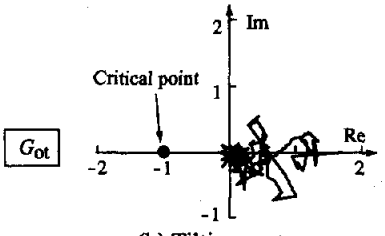

(b) Tilting system

FIGURE 15: Nyquist plot of open loop transfer function

5.7 Rotational test

A rotational test was performed by using the digital controller which was designed. Figure 16 shows the unbalanced response. The horizontal axis is rotational speed, and the vertical axis is the amplitude of the flexible rotor. The rotational speed was able to exceed the critical speed of Nc4 as a result of 4-plane balancing, and approached the critical speed of Nc5 as a result of 5-plane balancing. The operational rated speed of 250rps was reached without any instability or abnormal vibration.

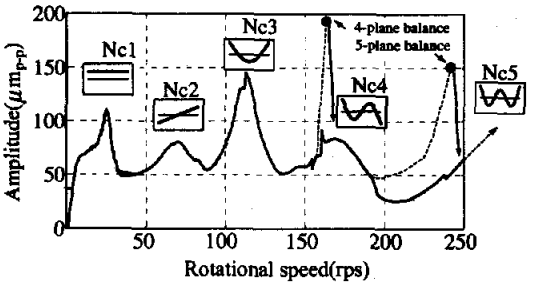

FIGURE 16: Rotational test (digital control)

6. CONCLUSION

By using analog control plus PBF, it is possible to successfully control high frequency vibration control through 1.5kHz in testing. However, a digital controller cannot realize these high frequency preformance because of sampling frequency.
To overcome the phase lag of digital control, two control modes were introduced (translating and tilting). The translating control employs the PID plus a notch filter and the tilting mode control installs the PID plus phase shifting filter. Through the use these filters, system stability is achieved. With respect to the stability margin, the latter is more recommended.
By using well tuned digital controllers, and a maximum five-plane balancing method employed, the rated speed of 250(rps) was achieved. Additionally two bending critical speeds were surpassed.

REFERENCE

1. Osami Matsushita, Trends in Active Magnetic Bearings, Tribologist, Vol.42, No.12, pp.972-997 1997 (In Japanese)
2. Naohiko TAKAHASHI, Osami MATSUSHITA, and Michiyuki TAKAGI, Control of Flexible Rotros Supported by Active Magnetic Bearing, Trans. of the Japan Soc. of Mech. Eng., 61-588, pp.3228-3233, 1995 (In Japanese)
3. Makoto ITO, Hiroyuki FUJIWARA, Hiroki OKUBO, and Osami MATSUSHITA, UNBALANCE VIBRATION CONTROL FOR HIGH ORDER BENDING CRITICAL SPEEDS OF FLEXIBLE ROTOR SUPPORTED BY ACTIVE MAGNETIC BEARINGS, Proc. of the 8th ISROMAC, March 2000